

Dark Energy and the Statistical Study of the Observed Image Separations of the Multiply Imaged Systems in the CLASS Statistical Sample

Abha Dev*, Deepak Jain †and Shobhit Mahajan

*Department of Physics and Astrophysics
University of Delhi, Delhi-110 007, India*

November 16, 2018

Abstract

The present day observations favour a universe which is flat, accelerated and composed of $\sim 1/3$ matter (baryonic + dark) and $\sim 2/3$ of a negative pressure component, usually referred to as dark energy or quintessence. The Cosmic Lens All Sky Survey (CLASS), the largest radio-selected galactic mass scale gravitational lens search project to date, has resulted in the largest sample suitable for statistical analysis. In the work presented here, we exploit observed image separations of the multiply imaged lensed radio sources in the sample. We use two different tests: (1) image separation distribution function $n(\Delta\theta)$ of the lensed radio sources and (2) $\Delta\theta_{\text{pred}}$ vs $\Delta\theta_{\text{obs}}$ as observational tools to constrain the cosmological parameters w and Ω_m . The results are in concordance with the bounds imposed by other cosmological tests.

1 Introduction

A number of observational tests strongly suggest that the universe is flat and the cosmological energy density includes a component that is not associated with matter – baryonic or dark. Results from distance measurements of type Ia supernovae (SNe Ia) combined with Cosmic Microwave Background Radiation (CMBR) observations [1, 2, 3, 4] and dynamic estimates of the quantity of matter in the universe seem to indicate that the simple picture provided by standard cold dark matter scenario is not enough [5]. These observations are often explained

*E-mail : abha@ducos.ernet.in

†At Deen Dayal Upadhyaya College, University of Delhi, Delhi 110015

by introducing a new hypothetical energy component, usually referred to as dark energy, with negative pressure. The dark energy is described by an ‘equation of state’ parameter w ($\equiv p_x/\rho_x$).

Since gravitational lensing takes place over cosmological distances, it can be used to measure the cosmological parameters. Various aspects of gravitational lensing have been studied and their use to probe the geometry and constitution of the universe has been investigated. The frequency of multiply imaged quasars is a sensitive function of the cosmological constant Λ and therefore the observed abundance of lensed quasars has been used to place upper bounds on Λ (Turner 1990 [6], Fukugita et al. 1992 [7], Kochanek 1996 [8]). The relation between the image separation $\Delta\theta$ and the source redshift z_S of multiply imaged quasars mostly depends on the sum of the matter density Ω_m and vacuum energy density Ω_Λ (Ω_i is the present density of the i^{th} component of the energy density relative to the present critical density; $\Omega_i \equiv \rho_{i0}/\rho_c$), and thus serves as a good indicator of the curvature of the universe. This aspect has been studied by Turner, Ostriker & Gott 1984 [9] Gott, Park & Lee 1989 [10], Fukugita et al. 1992 [7], Park & Gott 1997 [11], Williams [12] (1997) and more recently by Helbig (1998)[13]. Likelihood analysis of the flux limited samples (established by Kochanek 1996 [8]) is another way of obtaining constraints on the cosmological parameters. This method has been used extensively in recent times by many authors to find the permissible range of the parameters of the cosmological models (see for example, [8, 14, 15]). Image separation distribution function $n(\Delta\theta)$ has been used to study constraints on the cosmological parameters as well as on the properties of the galaxies [7, 16, 17, 18]. Yet another aspect of gravitational lensing statistics is the study of the mean image separation. Gott, Park & Lee (1989) [10] studied the mean image separation of images in cosmological models with a non-zero cosmological constant. Lee & Park (1994) (hereafter LP) [19], working with a sample of five multiply imaged quasars, used statistical methods to predict the best fit model. Their choice of models was restricted to six different combinations of parameters $(\Omega_m, \Omega_\Lambda)$.

In this work, we exploit the angular image separation of lensed quasars in two different ways to constrain the Ω_m and w :

- (i) We develop the image separation distribution function $n(\Delta\theta)$ of the multiply imaged lensed radio sources as a tool to perform quantitative analysis for finding the constraints on

the cosmological parameters w and Ω_m . We perform the chi-square test to put bounds on the parameters.

(ii) We calculate the expected value of the angular separation of a lensed radio source, $\Delta\theta_{\text{pred}}$ by averaging $\Delta\theta$ over the probability distribution function for its given redshift z_S , flux S_ν and redshift of the lensing galaxy z_L . To estimate the significance of the difference between the predicted and the observed $\Delta\theta$, we once again apply the chi-square test.

Radio source samples have several advantages over the optical quasar samples [20, 21]. Radio-selected sources are immune to extinction in the lens galaxy. They are also free from the systematic errors arising due to the fact that the lens galaxy has an apparent brightness comparable to that of the lensed images of the source. The resolution is much smaller than the typical image separation. The parent catalogues are in the form of large-area surveys from which unbiased samples can be selected and relatively easily observed. The Cosmic Lens All Sky Survey (CLASS) has resulted in the largest sample of radio sources suitable for statistical analysis [22, 15]. We adopt the CLASS statistical sample for our analyses. The sample consists of 8958 radio sources out of which 13 sources are multiply imaged. The sample had been selected so as to meet well defined observational selection criteria (see Browne et al.(2002)).

The statistical properties of gravitational lensing statistics are sensitive to the properties of galaxies (lenses) and the sources. It is thus important to use reliable galaxy luminosity functions (LFs) in the analysis of statistical lensing. We use the luminosity functions (LFs) for the early-type galaxies (i.e. ellipticals and S0 galaxies) and for the late-type galaxies (i.e. spirals and others) as provided by the recent large-scale observations of galaxies, particularly the Two Degree Field Galaxy Redshift Survey (2dfGRS) and the Sloan Digital Sky Survey (SDSS) [15].

The article is organized as follows: We begin Section 2 by listing the basic equations of gravitational lensing statistics and the assumptions we make to derive them. We also briefly describe the adopted source sample and luminosity function for the galaxies. In Section 3, we develop the image separation distribution function as a tool to put constraints on the cosmological parameters. Section 4 describes use of $\Delta\theta_{\text{pred}}$ vs $\Delta\theta_{\text{obs}}$ as a tool to constrain the parameters w and Ω_m . In Section 5 we discuss our findings.

2 Basic Equations and Assumptions

2.1 Cosmological Model, Distance Formula and Lookback Time

We consider a spatially flat, homogeneous and isotropic model of cosmology with non-relativistic matter with energy density ρ_m and a separately conserved “dark energy component” with an equation of state $p_x = w\rho_x$. The condition for a flat universe becomes $\Omega_m + \Omega_x = 1$ where

$$\Omega_m = \frac{8\pi G}{3H_0^2}\rho_{m0} \text{ and } \Omega_x = \frac{8\pi G}{3H_0^2}\rho_{x0}.$$

H_0 is the Hubble constant at the present epoch, while ρ_{m0} and ρ_{x0} are the non-relativistic matter density and the dark energy density respectively at the present epoch.

The age of the universe at a redshift z is given by

$$\begin{aligned} H_0 t(z) &= H_0 \int_z^\infty \frac{dz'}{(1+z')H(z')} \\ &= \int_z^\infty \frac{dz'}{(1+z')\sqrt{\Omega_m(1+z')^3 + \Omega_x(1+z')^{3(1+w)}}}. \end{aligned} \quad (1)$$

The angular diameter distance between objects at redshifts z_1 and z_2 is

$$d_A(z_1, z_2) = \frac{cH_0^{-1}}{(1+z_2)} \int_{z_1}^{z_2} \frac{dz}{\sqrt{\Omega_m(1+z)^3 + \Omega_x(1+z)^{3(1+w)}}}. \quad (2)$$

We adopt the notation $D_{LS} = d_A(z_L, z_S)$.

2.2 Galaxy Luminosity Function

The number density of galaxies with luminosities lying between L and $L + dL$ is assumed to be described by the Schechter function of the form [23]

$$\Phi(L, z=0)dL = \phi_* \left(\frac{L}{L_*}\right)^\alpha \exp\left(-\frac{L}{L_*}\right) \frac{dL}{L_*}, \quad (3)$$

where ϕ_* , α , and L_* are the characteristic number density, faint end slope and characteristic luminosity respectively at the present epoch. We further assume that the total comoving number density of galaxies is conserved. Thus the comoving number density of galaxies at redshift z is given by $n_L(z) = n_0(1+z)^3$ where n_0 is the present number density of galaxies.

Galaxy Type	α	γ	$v^*(\text{km/s})$	$\phi^*(\text{Mpc}^{-3})$	F^*
E/S0	-0.74	4.0	185	0.82×10^{-2}	0.014
S	-1.0	2.6	134	1.2×10^{-2}	0.008

Table 1: Lens and Schechter parameters for galaxies (for details see [15]).

The present day comoving number density of galaxies can be calculated as

$$n_0 = \int_0^\infty \Phi(L) dL. \quad (4)$$

The two large-scale galaxy surveys: 2dFGRS and SDSS, have produced converging results on the total LF. The surveys determined the Schechter parameters for galaxies (all types) at $z \leq 0.2$. Chae (2002) [15] has worked extensively on the information provided by the recent galaxy surveys to extract the local type-specific LFs. As the information on the total LF is abundant and the results are convergent, the total LF can be decomposed into an early-type LF and a late-type LF. The inference of the type-specific LFs from the total LF relies on an independent knowledge of relative type-specific LFs. We use the normalization corrected 2dFGRS lens and Schechter parameters as evaluated by Chae [15]. The 2dFGRS survey (Folkes et al. (1999) [24]) employs the “principal component analysis” of galaxy spectra, which essentially maximally quantify differences between the spectra of galaxies, to study LFs per type. Table 1 lists the lens and the Schechter parameters used in this work. We have adopted the parameters per morphological type as given by Chae (2002)[15].

For the ellipticals and lenticulars, characteristic velocity dispersion v_* and the characteristic luminosity L_* follow the Faber-Jackson relation ($L_* \propto v_*^{4.0}$). For spirals, v_* and L_* are related by the Tully-Fisher relation ($L_* \propto v_*^{2.6}$). We express this as

$$\frac{L}{L_*} = \left(\frac{v}{v_*}\right)^\gamma \quad (5)$$

with $\gamma = 4.0$ for the early-type galaxies and $\gamma = 2.6$ for the late-type.

2.3 Lensing Statistics

We consider the singular isothermal sphere (SIS) model for the lens mass distribution because of simplicity. SIS is a good approximation to the real mass distribution in galaxies [9, 16].

The cross-section for lensing events for the SIS lens is

$$\sigma = 16 \pi^3 \left(\frac{v}{c}\right)^4 \left(\frac{D_{OL} D_{LS}}{D_{OS}}\right)^2. \quad (6)$$

For the calculations presented here we ignore evolution of number density of galaxies and assume that the comoving number density is conserved. Under these assumptions, the differential probability of a lensing event by a galaxy with velocity dispersion v at redshift z_L is

$$d\tau = n_0 (1 + z_L)^3 \sigma \frac{cdt}{dz_L} dz_L. \quad (7)$$

The quantity cdt/dz_L in Friedman Robertson Walker (FRW) geometry for the adopted cosmological models is

$$\frac{cdt}{dz_L} = \frac{a_0}{(1 + z_L)} \frac{1}{\sqrt{\Omega_m (1 + z)^3 + \Omega_x (1 + z)^{3(1+w)}}} \quad (8)$$

where a_0 is the scale factor at the present epoch.

Substituting for σ from equation (6), we get

$$d\tau = n_0 (1 + z_L)^3 \frac{16\pi^3}{cH_0^3} v^4 \left(\frac{D_{OL} D_{LS}}{a_0 D_{OS}}\right)^2 \frac{1}{a_0} \frac{cdt}{dz_L} dz_L. \quad (9)$$

Using equations (4), (5) and (9), the differential optical depth of lensing in traversing dz_L with angular separation between ϕ and $\phi + d\phi$ is [7]:

$$\begin{aligned} \frac{d^2\tau}{dz_L d\phi} d\phi dz_L &= \frac{\gamma}{2\phi} \left[\frac{D_{OS}}{D_{LS}} \phi \right]^{\frac{\gamma}{2}(\alpha+1+\frac{4}{\gamma})} \exp \left[- \left(\frac{D_{OS}}{D_{LS}} \phi \right)^{\frac{\gamma}{2}} \right] \frac{cdt}{dz_L} \\ &\times F^* \frac{(1 + z_L)^3}{\Gamma \left(\alpha + \frac{4}{\gamma} + 1 \right)} \left[\left(\frac{D_{OL} D_{LS}}{a_0 D_{OS}} \right)^2 \frac{1}{a_0} \right] d\phi dz_L, \end{aligned} \quad (10)$$

where F^* is defined as

$$F^* = \frac{16\pi^3}{cH_0^3} \phi_* v_*^4 \Gamma \left(\alpha + \frac{4}{\gamma} + 1 \right). \quad (11)$$

The value of F^* for the adopted lens and Schechter parameters for the early and the late-type galaxies is given in Table 1.

2.4 The CLASS Statistical Sample

The sample consists of 8958 radio sources out of which 13 sources are multiply imaged. While using $n(\Delta\theta)$ as a tool to constrain the cosmological parameters, we work only with those multiply imaged sources whose image-splittings are known (or likely) to be caused by single galaxies. There are 9 such radio sources: 0218+357, 0445+123, 0631+519, 0712+472, 0850+054, 1152+199, 1422+231, 1933+503, 2319+051. (See Chae (2002) [15] for the complete and detailed list of the lensed sources.) We thus work with a total of 8954 radio sources. The sources probed by CLASS at $\nu = 5$ GHz are well represented by power-law differential number-flux density relation: $|dN/dS| \propto (S/S^0)^\eta$ with $\eta = 2.07 \pm 0.02$ (1.97 ± 0.14) for $S \geq S^0$ ($\leq S^0$) where $S^0 = 30$ mJy (McKean et al.(2002)). The redshift distribution of unlensed sources in the sample can be adequately described by a Gaussian model with a mean redshift $z = 1.27$ and dispersion of 0.95 [15]. Guided by the above information about (i) the number-flux density relation and (ii) the distribution of unlensed sources in redshift, we simulate the unlensed radio sources (8945 in number) of the CLASS statistical sample using the Monte-Carlo technique (rejection method).

2.5 Magnification Bias

Gravitational lensing causes a magnification of images and this transfers the lensed sources to higher flux density bins. In other words, the lensed quasars are over-represented in a flux-limited sample. The magnification bias $\mathcal{B}(z_S, S_\nu)$ increases the lensing probability significantly in a bin of total flux density (S_ν) by a factor

$$\mathcal{B}(z_S, S_\nu) = \left| \frac{dN_{z_S}(> S_\nu)}{dS_\nu} \right|^{-1} \int_{\mu_{min}}^{\mu_{max}} \left| \frac{dN_{z_S}(> S_\nu/\mu)}{dS_\nu} p(\mu) \right| \frac{1}{\mu} d\mu. \quad (12)$$

Here $N_{z_S}(> S_\nu)$ is the intrinsic flux density relation for the source population at redshift z_S . $N_{z_S}(> S_\nu)$ gives the number of sources at redshift z_S having flux greater than S_ν . For the SIS model, the magnification probability distribution is $p(\mu) = 8/\mu^3$. The minimum and maximum total magnifications μ_{min} and μ_{max} in equation (12) depend on the observational characteristics as well as the lens model. For the SIS model, the minimum total magnification is $\mu_{min} = 2$ and the maximum total magnification is $\mu_{max} = \infty$. For the CLASS statistical sample, one of selection criteria for the double-imaged systems is that the ratio of the flux

densities of the fainter to the brighter images \mathcal{R}_{min} is ≥ 0.1 . Given such an observational limit, the minimum total magnification for double imaging the adopted model of the lens is [15]:

$$\mu_{min} = 2 \frac{1 + \mathcal{R}_{min}}{1 - \mathcal{R}_{min}}. \quad (13)$$

The magnification bias \mathcal{B} depends on the differential number-flux density relation $|dN_{z_S}(> S_\nu)/dS_\nu|$. The differential number-flux relation needs to be known as a function of the source redshift. At present redshifts of only few CLASS sources are known. We, therefore, ignore redshift dependence of the differential number-flux density relation. Following Chae (2002) [15], we further ignore the dependences of the differential number-flux density relation on the spectral index of the source.

3 $n(\Delta\theta)$ As a Probe

The normalized image angular separation distribution for a source at z_S is obtained by integrating $\frac{d^2\tau}{dz_L d\phi}$ over z_L :

$$\frac{d\mathcal{P}}{d\phi} = \frac{1}{\tau(z_S)} \int_0^{z_S} \frac{d^2\tau}{dz_L d\phi} dz_L. \quad (14)$$

The corrected image separation distribution function for a single source at redshift z_S is given by [8, 17]

$$\begin{aligned} P'(\Delta\theta) &= \mathcal{B} \frac{\gamma}{2\Delta\theta} \int_0^{z_S} \left[\frac{D_{0S}}{D_{LS}} \phi \right]^{\frac{\gamma}{2}(\alpha+1+\frac{4}{\gamma})} \exp \left[- \left(\frac{D_{0S}}{D_{LS}} \phi \right)^{\frac{\gamma}{2}} \right] \\ &\times F^* \frac{cdt}{dz_L} \frac{(1+z_L)^3}{\Gamma(\alpha + \frac{4}{\gamma} + 1)} \left[\left(\frac{D_{OL}D_{LS}}{a_0 D_{OS}} \right)^2 \frac{1}{a_0} \right] dz_L. \end{aligned} \quad (15)$$

Similarly the corrected lensing probability for a given source at redshift z is given by [8, 17]

$$P' = \int \frac{d\mathcal{P}}{d\phi} \mathcal{B} d\phi. \quad (16)$$

Here ϕ and $\Delta\theta$ are related through $\phi = \frac{\Delta\theta}{8\pi(v^*/c)^2}$.

$\Delta\theta$ intervals: (arcseconds)	0.3 – 0.8	0.8 – 1.3	1.3 – 1.8	1.8 – 2.3	2.3 – 2.8	2.8 – 3.3
Number of lensed sources	2	4	3	0	0	0

Table 2: Observed distribution of the 9 multiply-imaged sources in the CLASS statistical sample.

The expected number of lensed radio sources is $n_L = \sum P'_i$, where P'_i is the lensing probability of the i^{th} source and the sum is over the entire adopted sample. Similarly, the image-separation distribution function for the adopted sample is $n(\Delta\theta) = \sum P'_i(\Delta\theta)$. The summation is over all the radio sources in the sample.

For the study of image separation distribution function, we neglect the contribution of spirals as lenses because their velocity dispersion is small as compared to ellipticals (Table 1).

For a given Ω_m and w , we compare the predicted number of multiply imaged sources in $\Delta\theta$ bins with the observed number of lensed radio sources in the corresponding bins. As one of the selection criteria for the multiply-imaged systems is that the compact radio core images have separations ≥ 0.3 arcseconds, we compare the image separation distributions for $\Delta\theta \geq 0.3$ arcseconds. Table 2 gives the observed image separation distribution of the multiply imaged radio sources. We perform the chi-square test to find bounds on w and Ω_m . We search for the combination (Ω_m, w) for which the value of chi-square becomes minimum. We define the chi-square as:

$$\chi^2 = \sum_{k=1}^6 \frac{(n_{\text{pred } k} - n_{\text{obs } k})^2}{n_{\text{obs } k}}. \quad (17)$$

Here $n_{\text{pred } k}$ is the predicted number of lensed sources with image separation in the interval corresponding to the k^{th} bin and is given by the area under the curve $n(\Delta\theta)$ for the bin under consideration. $n_{\text{obs } k}$ is the observed number of multiply imaged CLASS sources in the k^{th} bin. We work with the following ranges of the parameters: $-1 \leq w \leq 0$ and $0 \leq \Omega_m \leq 1$ and perform a grid search in the parametric space to find the best fit model. For the two parameter fit, the 68% Confidence Level (CL) (90% CL) corresponds to $\Delta\chi^2 = 2.3$ (4.61).

Source	$\Delta\theta_{\text{obs}}$ (arcseconds)	z_S	z_L	$\Delta\theta_{\text{pred}}$ (arcseconds) no sel.	$\Delta\theta_{\text{pred}}$ (arcseconds) sel.
0218+357	0.334	0.96	0.68	0.50	0.62
0712+472	1.27	1.34	0.41	1.19	1.26
1152+199	1.56	1.019	0.439	0.98	1.06
1422+231	1.28	3.62	0.34	1.56	1.62
1933+503	1.17	2.62	0.755	1.22	1.29
2319+051	1.36	2.0	0.624	1.18	1.26

Table 3: We take $z_S = 2$ for the source (2319+051) of unknown redshift, which is the mean redshift of the whole sample [15]. The fourth column gives the corresponding predicted image separations for the best fit model: $\Omega_m = 0$ & $w = -1$ when selection effects are not considered. The fifth column gives the predicted values of $\Delta\theta$ when selection effects are taken into account.

4 $\Delta\theta_{\text{pred}}$ vs $\Delta\theta_{\text{obs}}$ As an Observational Tool

With the lensing galaxy at redshift z_L , the mean image separation of images of a multiply imaged source at redshift z_S is given by [19]:

$$\Delta\theta_{\text{pred}} = \langle \Delta\theta \rangle = \frac{\sum \int \frac{d^2\tau}{dz_L d\Delta\theta} \Delta\theta d\Delta\theta}{\sum \int \frac{d^2\tau}{dz_L d\Delta\theta} d\Delta\theta}, \quad (18)$$

where the summation is over the galaxy types, E/S0 and S.

The expected dispersion of separation around the mean value is

$$\sigma_{\Delta\theta} = \sqrt{\langle \Delta\theta^2 \rangle - \langle \Delta\theta \rangle^2} \quad (19)$$

with

$$\langle \Delta\theta^2 \rangle = \frac{\sum \int \frac{d^2\tau}{dz_L d\Delta\theta} \Delta\theta^2 d\Delta\theta}{\sum \int \frac{d^2\tau}{dz_L d\Delta\theta} d\Delta\theta}. \quad (20)$$

We again focus our attention on the multiply imaged radio sources whose image-splittings are known (or likely) to be caused by single galaxies. Further, we consider only those lensed sources for which the source redshift z_S , redshift of the lensing galaxy z_L and observed image separation $\Delta\theta_{\text{obs}}$ are known. There are 6 such sources (Table 3).

We work with the following ranges of the parameters: $-1 \leq w \leq 0$ and $0 \leq \Omega_m \leq 1$. To find the best fit model we apply the chi-square test. The chi-square is defined as

$$\chi^2 = \sum_{i=1}^N \left[\frac{\Delta\theta_{\text{obs}\,i} - \Delta\theta_{\text{pred}\,i}}{\sigma_{\Delta\theta\,i}} \right]^2. \quad (21)$$

The sum is over all the data points ($N = 6$). The chi-square per degree of freedom for a two parameter fit is defined as $\chi_\nu^2 = \chi^2/(N-2)$. We perform a grid search in the parametric space to find the best fit model, the one for which value of χ^2 is minimum.

It is difficult to observe gravitational lens systems of multiple images having very small angular separations. As mentioned above (section 3), one of the selection criteria for the multiply-imaged system is that the compact radio core images have separations ≥ 0.3 arc-seconds. We, therefore, also work out the constraints tuned to this selection effect.

5 Results and Discussions

Image separation distribution function $n(\Delta\theta)$ has been used to study constraints on the cosmological parameters as well as on the properties of the galaxies [7, 16, 17, 18]. $n(\Delta\theta)$ is sensitive to the cosmological parameters via the angular diameter distance formula. Earlier work on $n(\Delta\theta)$ does not employ any statistical methods to put bounds on the parameters. As explained in section 3, we use the chi-square test to find the best fit model as well as the permissible range of w and the matter density Ω_m . It is interesting to note that χ^2 attains a minimum value of ~ 3.1893 (implying $\chi_{\nu\text{min}}^2 = 0.8$) for the combinations (Ω_m, w) , as indicated in Fig. 1. For these combinations the total number of lensed sources for the adopted sample, which is defined by the total area under the curve $n(\Delta\theta)$ vs $\Delta\theta$ (with $\Delta\theta \leq 3.3$), works out to be ~ 10.6 . Fig. 1 also shows the contours of 68% and 90% CL. The analysis provides us with the following constraints: $w \leq -0.13$ and $\Omega_m \leq 0.74$ at 68 % CL and $w \leq -0.05$ and $\Omega_m \leq 0.91$ at 90% CL.

Fig. 2 compares the observed distribution of the lensed sources in $\Delta\theta$ with the predicted distribution for $\Omega_m = 0.3$ and $w = -0.585$ (one of the points in the parametric space for which χ^2 is minimum).

The cosmological parameters determine the number of the predicted lensed sources in a bin and hence the height of the predicted histogram. There is, however, no shift in the peak

of the predicted histogram with the change in the values (Ω_m, w) . On the other hand, the location of the peak of the $n(\Delta\theta)$ curve strongly depends on the model of galaxy evolution [28, 29]. The tool developed in this piece of work can prove useful to study models of galaxy evolution. The image separation distribution function also depends on the mass profile of the lensing galaxies [30]. The above test can be used to suggest the preferred lens model or to constrain the parameters of the model under consideration.

In this article we also exploit the mean image separation as a tool to constrain the parameters Ω_m and w . The mean image separation of the multiply lensed quasar is sensitive to the parameters via the differential lensing probability.

It is interesting to note that the value of chi-square becomes minimum for $\Omega_m = 0.0$ and $w = -1$, with $\chi^2_{\nu \text{ min}} = 0.412$ (0.66) for the combination with no selection effects (with selection effects). This result is in agreement with the observations of Lee & Park [19]. They consider a flat universe with a non-zero cosmological constant and a sample of five gravitational lens systems. They report that among the six different models that they have considered, the ones with large Ω_Λ are preferred.

Fig. 3 shows the contour of 68% CL in the parametric space when ‘no selection effect’ is considered. The best-fit model for which the chi-square attains the minimum value is $\Omega_m = 0.0$ and $w = -1$. At 68 % CL, we get $\Omega_m \leq 0.5$ and $w \leq -0.24$. The entire parametric space is allowed at 90% CL.

Fig. 4 shows the results obtained when we incorporate the selection effects. The best fit model is again $\Omega_m = 0.0$ and $w = -1$. The constraints obtained are weaker when we take selection effects into account. The bounds are: $\Omega_m \leq 0.61$ and $w \leq -0.16$ at 68 % CL. The entire parametric space is allowed at 90 % CL.

The fourth and the fifth columns of Table 3 give the values of image separations as predicted by the best fit model. Like LP, we also observe that $\Delta\theta_{\text{pred}}$ is larger when selection effects are taken into account.

Table 4 lists the constraints obtained on w and Ω_m from various aspects of gravitational lensing statistics along with those obtained from other observational tests.

The observed statistical properties of gravitational lensing in a sample are the total rate of lensing, the lens redshifts, the source redshifts and the image multiplicity. In this body of work, we explored the use of image separation as an observational tool. The bounds obtained

in this article are concordant with those obtained from various other observational tests (see Table 4). Nevertheless, the constraints derived are exposed to the following possible sources of errors. We first point out those sources of errors which affect both the analyses.

(i) Like other aspects of gravitational lensing statistics, the observational tests presented here are sensitive to the lens and the Schechter parameters. At present, there is no consensus amongst the observationally derived results for early-type LF [15]. The main difficulty in the determination of the early-type LF lies in identifying a large number of galaxies by morphological types. In this piece of work we have used the current estimates of luminosity functions of galaxies per morphological type. The present derived constraints on the cosmological parameters are susceptible to systematic errors arising from the uncertainties in the early-type LF.

(ii) We adopt the SIS model for the lensing galaxies which is an over simplification.

(iii) In this work we work with the assumption that the early-type galaxies do not evolve with time. The presence of number evolution of galaxies in addition to pure luminosity evolution decreases the optical depth which makes the constraints on w weaker [27, 29]. The inclusion of the evolution factor also affects the image separation distribution [29].

The results of ‘ $n(\Delta\theta)$ test’ are further susceptible to the following sources of error:

- At present, redshifts of only a few CLASS sources are known and this affects the analysis in several ways. For instance, we are led to assume that the number-flux density relation of the radio sources in the CLASS statistical sample is independent of the source redshift z_S . This assumption adds to the possibility of an error. Further as Chae (2002) [15] has shown that the derived value of Ω_m (in a flat universe) is sensitive to the mean redshift. Thus there can be an error arising from the current uncertainty in the mean redshift.
- While using $n(\Delta\theta)$ as a probe we have ignored the use of spirals as lenses. This may be another possible source of error.

While using $\Delta\theta_{\text{pred}}$ vs $\Delta\theta_{\text{obs}}$ as a tool, we are led to work with a sample size of 6 multiply imaged radio sources. Availability of more data on the redshifts of the lenses and the radio sources as well as the lens parameters will help to use the tools described above in a more powerful way.

Method	Reference	w	Ω_m
Large scale structure +CMBR+SNe Ia data	Garnavich et al.[1], Perlmutter et al.[2] Efstathiou [3])	$w \leq -0.6$ at 95 % CL	$0.3 \leq \Omega_m \leq 0.4$ at 95 % CL
CMB	Spergel [4]	$w \leq -0.78$ at 95 % CL	$\Omega_m = 0.27 \pm 0.04$ at 95 % CL
Old High Redshift Galaxies	Lima and Alcaniz[25]	$w \leq -0.2$	$\Omega_m = 0.3$
Angular Size- Redshift Data	Lima and Alcaniz [26] (For $l \simeq 20h^{-1}Mpc$)	$w \leq -0.2$ at 68 % CL	$\Omega_m \leq 0.62$ at 68 % CL
X-ray Clusters of Galaxies	Schuecker et al. [31]	$w = -0.95^{+0.30}_{-0.35}$ at 1σ	$\Omega_m = 0.29^{+0.80}_{-0.12}$ at 1σ
Lensing Statistics (i) Likelihood Analysis	Waga and Miceli[14] (optical sample)	$w \leq -0.71$ at 68% CL	$0.24 \leq \Omega_m \leq 0.38$ at 68% CL
	Chae [15] (CLASS sample)	$w < -0.55^{+0.18}_{-0.11}$ at 68% CL	$\Omega_m = 0.31^{+0.27}_{-0.14}$ at 68% CL
(ii) $n(\Delta\theta)$	This paper (CLASS sample)	$w \leq -0.13$ at 68 % CL	$\Omega_m \leq 0.74$ at 68 % CL
(iii) $\Delta\theta_{\text{pred}}$ Vs $\Delta\theta_{\text{obs}}$	This Paper (CLASS sample)	$w \leq -0.24$ at 68 % CL	$\Omega_m \leq 0.5$ at 68 % CL

Table 4: Constraints on w & Ω_m from various cosmological tests.

Acknowledgement

We are thankful to Kyu -Hyun Chae, Phillip Helbig and Amber Habib for useful discussions. We also wish to thank Chris Kochanek, Lindsay King and Zong-Hong Zhu for their useful comments on the earlier version of the paper.

References

- [1] M. P. Garnavich et al., *Astrophys. J.*, **509**, 74 (1998).
- [2] S. Perlmutter et al., *Astrophys. J.*, **517**, 565 (1999).
- [3] G. Efstathiou, *Mon. Not. R. Astr. Soc.*, **310**, 842 (1999).
- [4] D. N. Spergel et al., **astro-ph/0302209** (2003).
- [5] M. S. Turner, *Physica Scripta*, **T85**, 210 (2000).
- [6] E. L. Turner, *Astrophys. J.*, **365**, L43 (1990).
- [7] M. Fukugita, K. Futamase, M. Kasai & E. L. Turner, *Astrophys. J.*, **393**, 3 (1992).
- [8] C. S. Kochanek, *Astrophys. J.*, **466**, 638 (1996a) [**K96**].
- [9] E. L. Turner, J. P. Ostriker & J. R. Gott III, *Astrophys. J.*, **284**, 1 (1984) [**TOG**].
- [10] J. R. Gott III, M. G. Park & M. H. Lee, *Astrophys. J.*, **338**, 1 (1989).
- [11] M. G. Park & J. R. Gott III, *Astrophys. J.*, **489**, 476 (1997).
- [12] L. L. R. Williams, *Mon. Not. R. Astr. Soc.*, **292**, L27 (1997).
- [13] P. Helbig, *Mon. Not. R. Astr. Soc.*, **298**, 395 (1998).
- [14] I. Waga & A. P. M. R. Miceli, *Phys. Rev. D.*, **59**, 103507 (1999).
- [15] K. H. Chae, **astro-ph/0211244**.
- [16] D. Maoz & H. W. Rix, *Astrophys. J.*, **416**, 425 (1993) [**MR**].

- [17] M. Chiba & Y. Yoshii, *Astrophys. J.*, **510**, 42 (1999).
- [18] D. Jain et al., *Int. J. Mod. Phys. D* **12**, 953 (2003).
- [19] M. H. Lee & M. G. Park, *J. Of The Korean Astronomical Society*, **27**, 103 (1994) [**LP**].
- [20] E. Falco, C. S. Kochanek & J. A. Muñoz, *Astrophys. J.*, **494**, 47 (1998).
- [21] P. Helbig et al., *Astr. Astrophys.*, **136**, 297 (1999).
- [22] S. T. Myers et al., *Mon. Not. R. Astr. Soc.*, (in press) (2002); I. W. A. Browne et al., *Mon. Not. R. Astr. Soc.*, (in press) (2002); D. R. Marlow, et al., *Astronom. J.*, **119**, 2629 (2000); I. Waddington et al., *Mon. Not. R. Astr. Soc.*, **328**, 882 (2001); J. S. Dunlop & J. A. Peacock, *Mon. Not. R. Astr. Soc.*, **247**, 19 (1990).
- [23] P. Schechter, *Astrophys. J.*, **203**, 297 (1976).
- [24] S. Folkes et al., *Mon. Not. R. Astr. Soc.*, **308**, 459 (1999).
- [25] J. A. S. Lima & J. S. Alcaniz, *Mon. Not. R. Astr. Soc.*, **317**, 893 (2000).
- [26] J. A. S. Lima & J. S. Alcaniz, **astro-ph/0109047**.
- [27] D. Jain, N. Panchapakesan, S. Mahajan & V. B. Bhatia, *Int. J. Mod. Phys. A*, **13**, 4227 (1998).
- [28] D. Jain, N. Panchapakesan, S. Mahajan & V. B. Bhatia, *Mod. Phys. Lett. A*, **15**, 41 (2000).
- [29] A. Dev et al., *Int. J. Mod. Phys. D*, **12**, 101 (2003).
- [30] D. Huterer & C. P. Ma, **astro-ph/0307301**.
- [31] P. Schuecker et al., *Astr. Astrophys.*, **402**, 53 (2003).

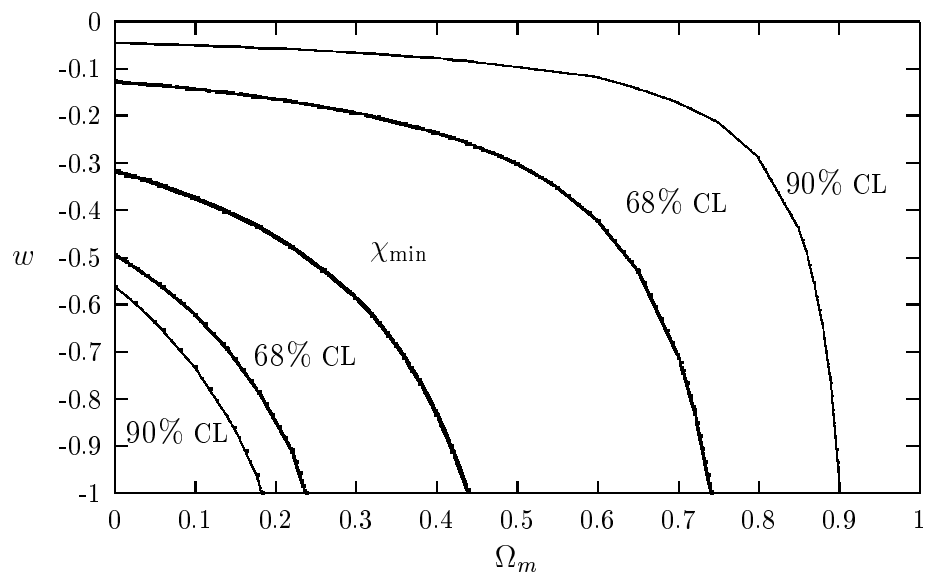


Figure 1: The contours showing permissible region of the parametric space within 68% CL and 90% CL. The contour labeled χ_{\min} corresponds to those combinations of Ω_m and w for which the value of chi-square is minimum.

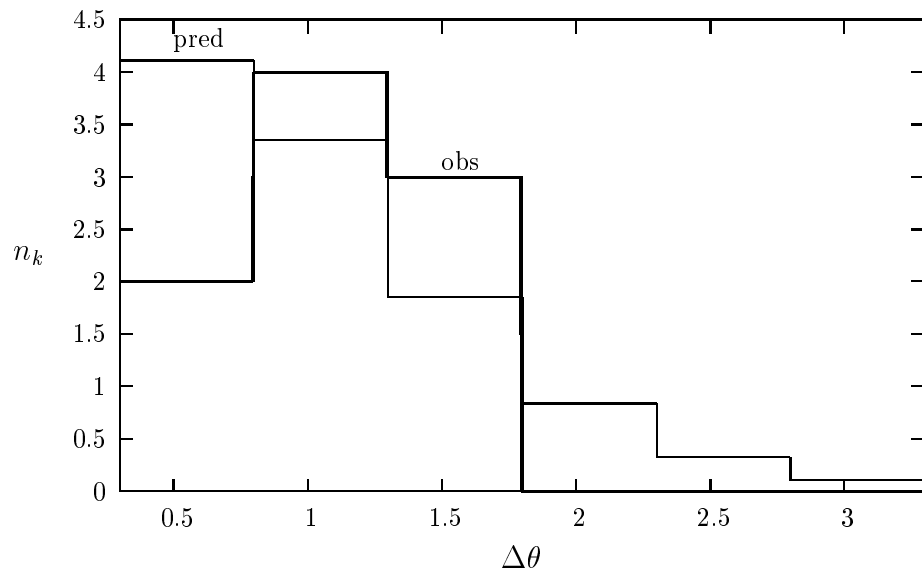


Figure 2: The observed distribution of lensed radio sources in $\Delta\theta$ vs the predicted distribution for $\Omega_m = 0.3$ and $w = -0.585$.

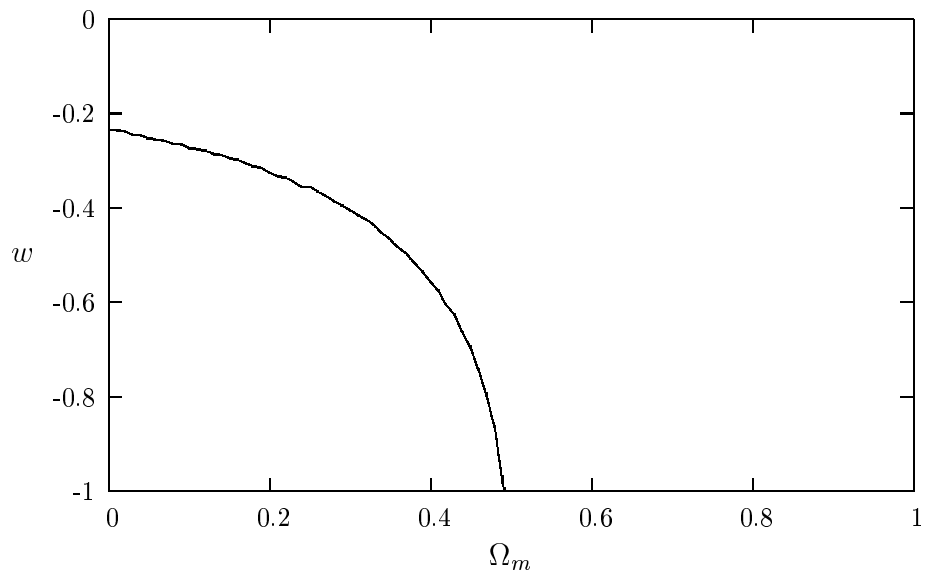


Figure 3: Results of $\Delta\theta_{\text{pred}}$ Vs $\Delta\theta_{\text{obs}}$ test. The graph shows the permissible region of Ω_m - w plane when selection effect is not considered. The contour corresponds to 68% CL, the best fit model being: $\Omega_m = 0$ with $w = -1$. The contour corresponding to 90% CL lies outside the range chosen for (Ω_m, w)

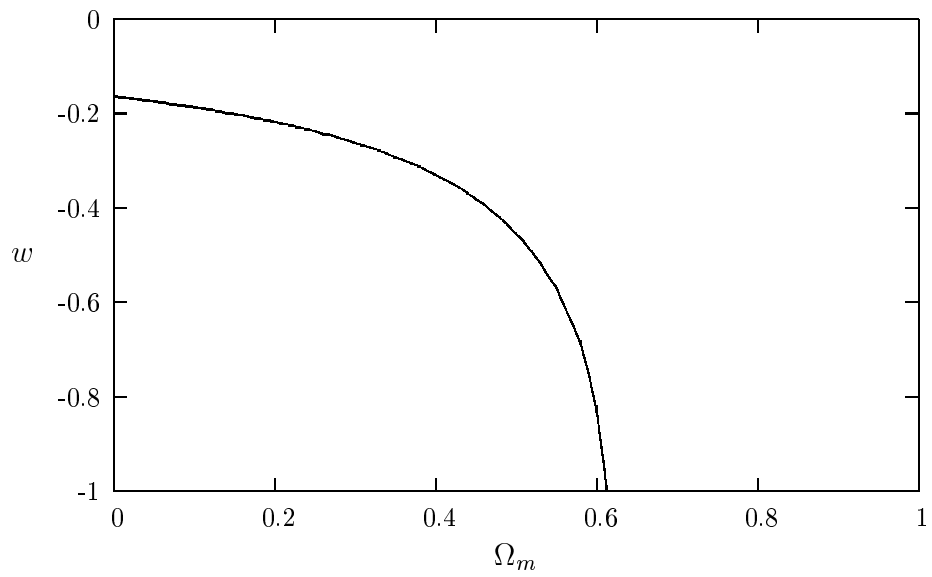


Figure 4: Results of $\Delta\theta_{\text{pred}}$ Vs $\Delta\theta_{\text{obs}}$ test. The graph shows the permissible region of Ω_m - w plane when selection effect is taken into account. The contour corresponds to 68% CL, the best fit model being: $\Omega_m = 0$ with $w = -1$. The contours corresponding to 90% CL lies outside the range chosen for (Ω_m, w)